

Mononuclear Organometallic Pd(II), Pd(III), and Pd(IV) Complexes Stabilized by a Pyridinophane Ligand with a C-Donor Group

Nicholas P. Ruhs,[‡] Julia R. Khusnutdinova,[§] Nigam P. Rath,^{||} and Liviu M. Mirica^{*,†}

[†]Department of Chemistry, University of Illinois at Urbana–Champaign, 600 S. Mathews Avenue, Urbana, Illinois 61801, United States

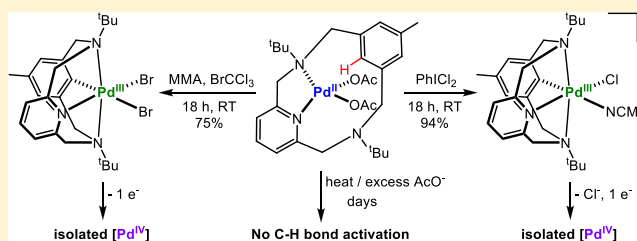
[‡]Department of Chemistry, Washington University in St. Louis, One Brookings Drive, St. Louis, Missouri 63130-4899, United States

[§]Okinawa Institute of Science and Technology Graduate University, Coordination Chemistry and Catalysis Unit, 1919-1 Tancha, Onna-son, Okinawa 904-0495, Japan

^{||}Department of Chemistry and Biochemistry, One University Boulevard, University of Missouri-St. Louis, St. Louis, Missouri 63121-4400, United States

Supporting Information

ABSTRACT: A series of Pd complexes bearing modified tetradentate pyridinophane ligands ^RN₃CH, containing a C-donor phenyl group, were isolated and characterized. The (^RN₃CH)Pd^{II}(OAc)₂ complexes contain a C_{ipso}–H bond that remains unactivated at the Pd^{II} stage, even upon heating or addition of excess acetate. These Pd^{II}(OAc)₂ complexes exhibit catalytic reactivity in the Kharasch radical addition of bromotrichloromethane to methyl methacrylate. Interestingly, novel Pd^{III} complexes (^RN₃C)Pd^{III}Br₂ were isolated from the Kharasch reaction mixture and have been characterized by EPR, UV–vis spectroscopy, and X-ray crystallography, suggesting that activation of the C_{ipso}–H bond has occurred during the oxidative conditions of the Kharasch radical addition. Inspired by this observation, several (^{PMe}N₃C)Pd^{III} complexes were synthesized upon oxidation of the Pd^{II} precursors with PhICl₂ and subsequent halide abstraction with thallium salts. Furthermore, additional one-electron oxidation generates detectable Pd^{IV} species, including an uncommon tricationic [(^{PMe}N₃C)Pd^{IV}(MeCN)₃]³⁺ complex. Overall, these initial results show that the ^RN₃C(H) ligand system is capable of stabilizing high-valent Pd species that can undergo uncommon oxidative and catalytic reactivity, including C–H bond activation.



INTRODUCTION

The involvement of Pd⁰ and Pd^{II} intermediates in palladium-catalyzed reactions has been extensively studied and documented over the past several decades.^{1,2} More recently, Pd^{III} and Pd^{IV} complexes have been implicated as active intermediates in many oxidative transformations.^{3–11} Studies have suggested that these high-valent Pd complexes have particular applicability in transformations involving C–H bond functionalization to form new C–X bonds (X = OAc, OH, halide, etc.).^{12–16} However, while there are numerous reports that support the occurrence of C–H bond activation at the Pd^{II} oxidation state, and even at Pd^{IV} centers,^{17,18} to our knowledge, there are no known reports that implicate the involvement of a Pd^{III} intermediate in the C–H activation of organic substrates.

Recently, NCN pincer ligands have been reported to form stable complexes with palladium via C–H bond activation of the C_{aryl}–H bond in the NCN moiety.^{19,20} Furthermore, our group has recently reported the characterization of Pd^{III} complexes stabilized by the *N,N'*-dialkyl-2,11-diaza[3.3](2,6)-pyridinophane (^RN₄, R = ^tBu, ⁱPr, Me) ligands and we have studied their reactivity in C–C and C–heteroatom bond

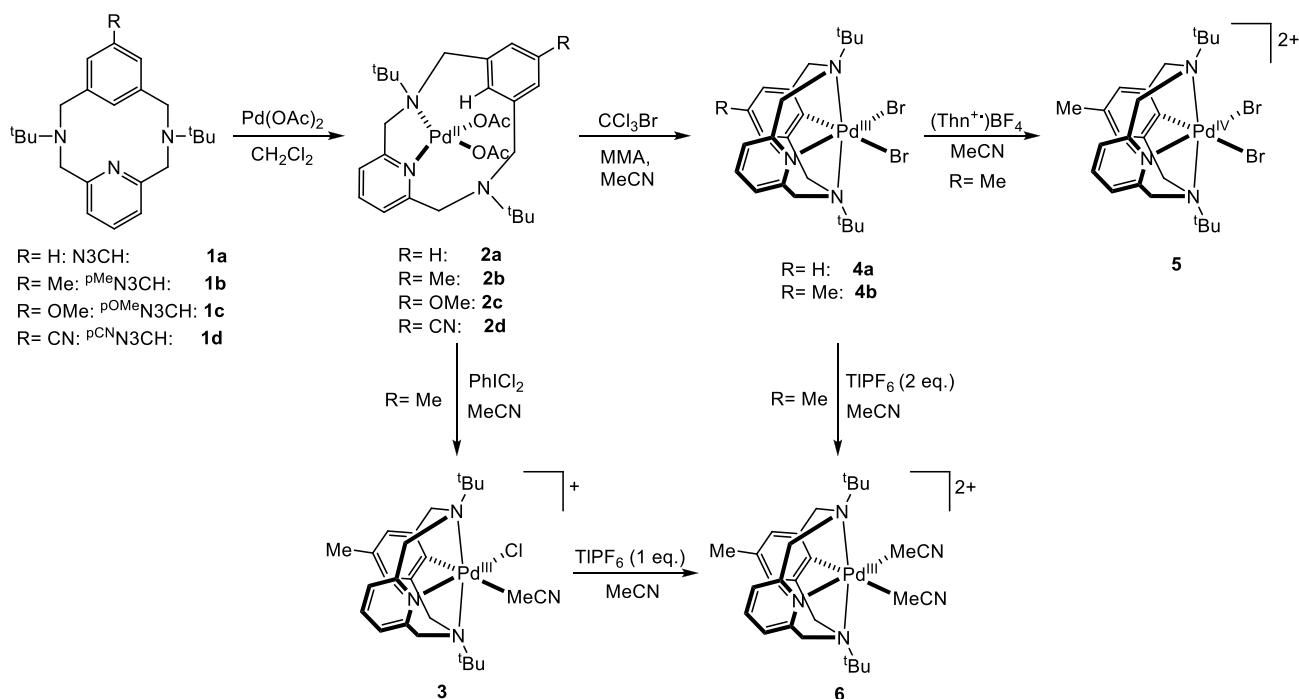
formation reactions and proposed mechanisms involving high-valent Pd^{III} and Pd^{IV} intermediates in such transformations.^{11,21,22}

In order to further expand the reactivity of high-valent Pd species, we sought out to employ a modified pyridinophane ligand system, ^RN₃CH, which contains a phenyl donor group and thus combines the features of the ^RN₄ and NCN pincer ligands.^{23–26} Reported herein is the synthesis, characterization, and reactivity of a series of Pd^{II}, Pd^{III}, and Pd^{IV} complexes supported by the ligands ^PR^RN₃CH (R = H, Me, OMe, CN) with different *para* substituents on the phenyl ring (Scheme 1). Interestingly, the ^RN₃CHPd(OAc)₂ complexes **2a–d** do not undergo C_{aryl}–H bond activation at the Pd^{II} stage, even upon heating or treatment with excess acetate. Moreover, these complexes can act as catalysts in the Kharasch radical addition of bromotrichloromethane (CCl₃Br) to methyl methacrylate (MMA), which surprisingly results in the formation of C–H activated Pd^{III} complexes ^RN₃CPd^{III}Br₂ (**4a,b**, Scheme 1), which were structurally and spectroscopically characterized.

Received: July 26, 2019

Published: September 24, 2019



Scheme 1. Synthesis of $(^R\text{N}3\text{C})\text{Pd}^{\text{III}}$ and $(^R\text{N}3\text{C})\text{Pd}^{\text{IV}}$ Complexes

Several $(^{\text{pMe}}\text{N}3\text{C})\text{Pd}^{\text{III}}$ complexes were synthesized upon oxidation of Pd^{II} precursors with PhICl_2 and subsequent halide abstraction with thallium salts. Furthermore, additional one-electron oxidation of these Pd^{III} systems generated detectable Pd^{IV} species, including an uncommon tricationic $[(^{\text{pMe}}\text{N}3\text{C})\text{Pd}^{\text{IV}}(\text{MeCN})_3]^{3+}$ complex. Overall, these initial results show that the $^R\text{N}3\text{C}(\text{H})$ ligand system is capable of stabilizing high-valent Pd species that can undergo unique oxidative and catalytic reactivity, including C–H bond activation.

EXPERIMENTAL DETAILS

General Specifications. All operations were performed under a nitrogen atmosphere using standard Schlenk and glovebox techniques if not indicated otherwise. All reagents for which the syntheses are not given were purchased from Sigma-Aldrich, Acros, STREM, or Pressure Chemical and were used as received without further purification. Solvents were purified prior to use by passing through a column of activated alumina using an MBRAUN SPS. The $^{\text{pH}}\text{N}3\text{CH}$ and $^{\text{pOMe}}\text{N}3\text{CH}$ ligands were synthesized following previously published procedures.^{23–26} NMR spectra were obtained on a Varian Mercury-300 spectrometer (300.121 MHz) or a Varian Unity Inova-500 spectrometer (500 MHz). Chemical shifts are reported in parts per million (ppm) with residual solvent resonance peaks as internal references. Abbreviations for the multiplicity of NMR signals are singlet (s), doublet (d), triplet (t), quartet (q), multiplet (m), and broad resonance (br). Solution magnetic susceptibility measurements for Pd^{III} complexes were obtained at 293 K by the Evans method²⁷ using coaxial NMR tubes and CD_3CN , and the corresponding diamagnetic corrections were included.²⁸ UV–visible spectra were recorded on a Varian Cary 50 Bio spectrophotometer and are reported as λ_{max} nm (ϵ , $\text{M}^{-1} \text{cm}^{-1}$). EPR spectra were recorded on a Bruker EMX-PLUS EPR or a JEOL JES-FA EPR spectrometer at X-band (9.2 GHz) in 3:1 PrCN:MeCN at 77 K. The purchase of the Bruker EMX-PLUS EPR spectrometer was supported by the National Science Foundation MRI program (NSF-MRI CHE-1429711). ESI-MS experiments were performed using a linear quadrupole ion trap Fourier transform ion cyclotron resonance mass spectrometer (LTQ-FTMS, Thermo, San Jose, CA) or a Bruker Maxis Q-TOF mass

spectrometer with an electrospray ionization source. ESI mass spectrometry was provided by the Washington University Mass Spectrometry Resource. Elemental Analysis was carried out by Intertek Pharmaceutical Services. Cyclic voltammetry (CV) studies were performed with a BASi EC Epsilon electrochemical workstation or CHI Electrochemical Analyzer 660D. Electrochemical grade Bu_4NClO_4 from Fluka was used as the supported electrolyte. The electrochemical measurements were performed under a blanket of nitrogen, and the analyzed solutions were deaerated by purging with nitrogen. A glassy carbon disk electrode (GCE, 1.6 mm diameter) was used as the working electrode, and a Pt wire as the auxiliary electrode. The nonaqueous Ag-wire reference electrode assembly was filled with 0.01 M $\text{AgNO}_3/0.1 \text{ M Bu}_4\text{NClO}_4/\text{MeCN}$ solution. The reference electrodes were calibrated against ferrocene (Fc) during each CV experiment.

Preparation of $^{\text{pMe}}\text{N}3\text{CH}$ (1b). A solution of bis[(*N*-*t*-butylamino)methyl]pyridine²⁹ (4.39 g, 17.6 mmol) in benzene (70 mL) and a 10% Na_2CO_3 aqueous solution (90 mL) was charged into a three-neck 500 mL round-bottom flask equipped with an addition funnel and a magnetic stirring bar. The reaction mixture was stirred and heated to 70 °C under a N_2 atmosphere, after which 3,5-bis(bromomethyl)toluene (3.3835 g, 12.2 mmol) in benzene (80 mL) was added dropwise to the reaction mixture over 1 h. The biphasic mixture was stirred at 70 °C overnight. Upon cooling to room temperature, the aqueous and benzene layers were separated. The benzene layer was washed with concentrated K_2CO_3 (3 × 50 mL) and subsequently dried over MgSO_4 . The organic layer was then filtered and evaporated to give a crude white solid. The crude white solid was heated at reflux in hot heptane (50 mL) for 2 h, and the resulting suspension was vacuum filtered. The heptane filtrate was evaporated to dryness, and the solid was redissolved in hot heptane (40 mL). After heating for 1 h, the resulting suspension was filtered, and the heptane filtrate was cooled to –20 °C overnight. The resulting white crystalline precipitate was vacuum filtered and subsequently dissolved in toluene (10 mL) at 90 °C, and the solution was filtered through a cotton plug. The toluene filtrate was cooled to +4 °C for 3 h. The white crystalline solid corresponding to $^{\text{pMe}}\text{N}3\text{CH}$ (625.5 mg) was collected and dried. A second fraction of $^{\text{pMe}}\text{N}3\text{CH}$ was obtained by cooling the toluene filtrate at –20 °C overnight. The second crop of white crystalline solid was collected and dried (162.9 mg). Total yield: 788.8 mg (18%). ^1H NMR (300 MHz, CDCl_3), δ : 1.32 (s, 18H,

tBu), 2.06 (s, 3H, Ph-CH₃), 3.74–3.89 (br d, 8H, –CH₂–), 6.49 (s, 2H, Ph-H), 6.69 (d, 2H, Py-H), 7.04 (s, 1H, Ph-H), 7.08 (t, 1H, Py-H).

Preparation of ^pCN³CH (1d). (1) *Synthesis of 4-bromo-3,5-bis(bromomethyl)benzonitrile.* A 250 mL round-bottom flask equipped with a magnetic stirring bar was charged with 4-bromo-3,5-dimethylbenzonitrile (0.20 g, 0.95 mmol, 1 equiv), NBS (0.68 g, 3.82 mmol, 4 equiv), and AIBN (0.08 g, 0.48 mmol, 0.5 equiv) under N₂, and 50 mL of DCM was added. The reaction was stirred at room temperature for 24 h under N₂. The solvent was removed and the solid was extracted with Et₂O (3 × 50 mL). The reaction mixture was purified via flash chromatography (hexanes/ethyl acetate), and the product was isolated as a white powder (yield: 87 mg, 25%). ¹H NMR (300 MHz, CDCl₃), δ: 7.69 (s, 2H, Ar), 4.62 (s, 4H, CH₂). ¹³C NMR (100.5 MHz, CDCl₃): 140.4, 134.0, 131.9, 117.1, 112.6, 32.1. (2) *Synthesis of ^pCN³CH (1d).* A 250 mL three-neck round-bottom flask equipped with a reflux condenser, an addition funnel, and a magnetic stirring bar was charged with a solution of N,N'-(pyridine-2,6-diylbis(methylene))bis(2-methylpropan-2-amine) (0.60 g, 2.40 mmol, 1 equiv) in 100 mL of toluene and 60 mL of 40% aqueous solution of Na₂CO₃. The stirred reaction mixture was preheated on an oil bath at 90 °C. A solution of 4-bromo-3,5-bis(bromomethyl)benzonitrile (0.89 g, 2.40 mmol, 1 equiv) in 20 mL of toluene was added dropwise to the stirred reaction mixture over 2 h. The resulting solution was heated at 95 °C under N₂ for an additional 12 h. The reaction mixture was cooled down to RT, the organic layer was separated and dried, and the solvent was removed in vacuo to generate a white solid. The white solid was dissolved into 4 mL of DCM and layered with 16 mL of pentane to yield the desired product as white crystals overnight (yield: 880 mg, 82%). ¹H NMR (500 MHz, CDCl₃), δ: 7.28 (t, 1H, Ar), 7.05 (s, 2H, Ar), 6.79 (d, 2H, Ar), 4.18–4.14 (m, 4H, CH₂), 4.06 (d, 2H, CH₂), 3.48 (d, 2H, CH₂), 1.32 (s, 18H, CH₃). ¹³C NMR (100.5 MHz, CDCl₃), δ: 159.9, 141.0, 135.5, 134.4, 121.9, 120.7, 118.9, 109.8, 57.0, 56.3, 54.3, 27.9. ESI-MS in MeCN: m/z 455.1801 (calcd for [^pCN³CH-H]⁺, C₂₄H₃₂BrN₄, m/z 455.1805).

Preparation of N3CHPd^{II}(OAc)₂ (2a). In a 100 mL round-bottom flask equipped with a stir bar, N3CH (48.1 mg, 0.137 mmol) and Pd(OAc)₂ (30.7 mg, 0.137 mmol) were dissolved in CH₂Cl₂ (15 mL). The resulting orange solution was stirred at room temperature under N₂ in the dark for 6 h. The dichloromethane was evaporated, and the orange residue was triturated with diethyl ether. A yellow precipitate was collected via vacuum filtration, washed with diethyl ether and pentane, and dried under vacuum. Yield: 61.7 mg (78%). ¹H NMR (300 MHz, CDCl₃), δ: 1.29 (s, 9H, tBu-CH), 1.33 (s, 3H, tBu-CH), 1.39 (s, 3H, tBu-CH), 1.63 (s, 3H, OAc-H), 1.82 (s, 3H, OAc-H), 2.22 (s, 3H, tBu-CH), 3.42 (d, 1H, –CH₂–), 3.72 (d, 1H, –CH₂–), 3.81 (m, 2H, –CH₂–), 4.29 (d, 1H, –CH₂–), 4.39 (d, 1H, –CH₂–), 4.65 (d, 1H, –CH₂–), 5.16 (d, 1H, –CH₂–), 6.70 (d, 1H, Py-H_{meta}), 6.76 (d, 1H, Py-H_{meta}), 6.79 (t, 1H, Ph-H_{para}), 6.91 (d, 1H, Ph-H_{para}), 6.98 (d, 1H, Ph-H_{meta}), 7.37 (t, 1H, Py-H_{para}), 11.09 (s, 1H, Ph-H_{ipso}). ¹³C NMR (100.5 MHz, CDCl₃), δ: 181.4, 180.2, 169.9, 161.6, 139.1, 138.6, 137.4, 135.2, 133.3, 131.6, 129.2, 125.1, 117.6, 69.1, 65.0, 62.9, 58.3, 58.0, 56.3, 30.5, 26.4, 25.3. Anal. Found: C, 55.09; H, 6.75; N, 7.01. Calculated for C₂₉H₄₃N₃O₆Pd·HOAc: C, 54.76; H, 6.81; N, 6.61.

Preparation of ^pMeN3CHPd^{II}(OAc)₂ (2b). In a 100 mL round-bottom flask equipped with a stir bar, ^pMeN3CH (167.0 mg, 0.457 mmol) and Pd(OAc)₂ (102.6 mg, 0.457 mmol) were dissolved in CH₂Cl₂ (50 mL). The resulting orange solution was stirred at room temperature under N₂ in the dark for 6 h. The dichloromethane was evaporated, and the orange residue was triturated with diethyl ether. A yellow precipitate was collected via vacuum filtration, washed with diethyl ether and pentane, and dried under vacuum. Yield: 229 mg (85%). ¹H NMR (300 MHz, CDCl₃), δ: 1.29 (s, 9H, tBu-CH), 1.32 (s, 3H, tBu-CH), 1.38 (s, 3H, tBu-CH), 1.85 (s, 3H, OAc-H), 1.97 (s, 3H, OAc-H), 2.06 (s, 3H, Ph-CH₃), 2.27 (s, 3H, tBu-CH), 3.18 (d, 1H, –CH₂–), 3.48 (d, 1H, –CH₂–), 3.80 (m, 2H, –CH₂–), 4.17 (d, 1H, –CH₂–), 4.30 (d, 1H, –CH₂–), 4.73 (d, 1H, –CH₂–), 5.03 (d, 1H, –CH₂–), 6.37 (d, 2H, Py-H_{meta}), 6.52 (d, 1H, Ph-H), 6.96 (d,

1H, Ph-H), 7.21 (t, 1H, Py-H_{para}), 10.64 (s, 1H, Ph-H_{ipso}). ¹³C NMR (100.5 MHz, CDCl₃), δ: 181.6, 180.1, 170.9, 162.7, 140.2, 138.1, 137.9, 136.0, 134.0, 127.2, 118.3, 69.8, 65.5, 63.1, 58.5, 58.2, 57.1, 30.4, 26.3, 25.4, 23.3. Anal. Found: C, 56.59; H, 6.82; N, 6.83. Calculated for C₂₈H₄₁N₃O₄Pd: C, 56.99; H, 7.00; N, 7.12.

Preparation of ^pMeN3CHPd^{II}(OAc)₂ (2c). In a 100 mL round-bottom flask equipped with a stir bar, ^pMeN3CH (24.6 mg, 0.064 mmol) and Pd(OAc)₂ (14.5 mg, 0.064 mmol) were dissolved in CH₂Cl₂ (10 mL). The resulting orange solution was stirred at room temperature under N₂ in the dark for 6 h. The dichloromethane was evaporated, and the orange residue was triturated with diethyl ether. A yellow precipitate was collected via vacuum filtration, washed with diethyl ether and pentane, and dried under vacuum. Yield: 29.5 mg (75%). ¹H NMR (300 MHz, CDCl₃), δ: 1.30 (s, 18H, tBu-CH), 2.28 (s, 3H, Ph-CH₃), 3.16 (d, 1H, –CH₂–), 3.58 (s, 3H, OMe-H), 3.77–3.84 (m, 3H, –CH₂–), 4.17 (s, 1H, –CH₂–), 4.30 (s, 1H, –CH₂–), 4.72 (s, 1H, –CH₂–), 5.08 (s, 1H, –CH₂–), 6.20 (d, 2H, Py-H_{meta}), 6.47 (d, 1H, Ph-H), 7.02 (d, 1H, Ph-H), 7.22 (t, 1H, Py-H_{para}), 10.47 (s, 1H, Ph-H_{ipso}). Anal. Found: C, 55.17; H, 6.82; N, 6.83. Calculated for C₂₈H₄₁N₃O₄Pd: C, 55.49; H, 6.82; N, 6.93.

Preparation of ^pCN³CHPd^{II}(OAc)₂ (2d). In a 100 mL round-bottom flask equipped with a stir bar, ^pCN³CH (43.4 mg, 0.115 mmol) and Pd(OAc)₂ (25.9 mg, 0.115 mmol) were dissolved in CH₂Cl₂ (15 mL). The resulting orange solution was stirred at room temperature under N₂ in the dark for 6 h. The dichloromethane was evaporated, and the orange residue was triturated with diethyl ether. A yellow precipitate was collected via vacuum filtration, washed with diethyl ether and pentane, and dried under vacuum. Yield: 28 mg (41%). ¹H NMR (300 MHz, CDCl₃), δ: 1.32 (s, 18H, tBu-CH), 2.32 (s, 3H, Ph-CH₃), 3.26 (d, 1H, –CH₂–), 3.45 (d, 1H, –CH₂–), 3.86–3.93 (m, 2H, –CH₂–), 4.26–4.37 (m, 2H, –CH₂–), 4.79 (d, 1H, –CH₂–), 5.11 (d, 1H, –CH₂–), 6.54 (d, 1H, Py-H_{meta}), 6.91 (s, 1H, Ph-H_{meta}), 7.03 (d, 1H, Py-H_{meta}), 7.12 (s, 1H, Ph-H_{meta}), 7.35 (t, 1H, Py-H_{para}), 11.41 (s, 1H, Ph-H_{ipso}). Anal. Found: C, 53.62; H, 5.72; N, 8.82. Calculated for C₂₈H₃₈N₄O₄Pd·1/2CH₂Cl₂: C, 53.19; H, 6.11; N, 8.71.

Preparation of [^pMeN3CPd^{III}(Cl)MeCN](ClO₄) (3). To a solution of ^pMeN3CHPd^{II}(OAc)₂ (47.3 mg, 0.080 mmol) in MeCN (1.5 mL) was added PhICl₂ (22.0 mg, 0.080 mmol) in MeCN (0.5 mL). The reaction mixture was stirred for 20 min, during which time the solution changed from a light orange to a dark green color. The solution was filtered, LiClO₄ (25.6 mg, 0.080 mmol) was added to the filtrate, and the solution was stirred for an additional 20 min. The resulting dark green solution was filtered and diethyl ether was added to the solution, causing the precipitation of a dark green solid. The product was collected via vacuum filtration and dried. Yield: 40 mg (94%). UV–vis, λ, nm (ε, M⁻¹, cm⁻¹), MeCN: 638 (551), 473 (548), 355 (1565). Anal. Found: C, 47.80; H, 5.78; N, 8.44. Calculated for C₂₆H₃₇Cl₂N₄O₄Pd: C, 48.27; H, 5.77; N, 8.66.

Preparation of ^pMeN3CPd^{III}Br₂ (4b): Kharasch Radical Addition. In a 20 mL vial equipped with a small magnetic stir bar, ^pMeN3CHPd^{II}(OAc)₂ (150 mg, 0.254 mmol) was dissolved in MeCN (10 mL) and stirred. To the stirring orange solution was added methyl methacrylate (250 μL, 2.35 mmol) and bromotrichloromethane (1.20 mL, 12.2 mmol). The solution changed from a dark orange color to a dark green color over 30 min. The reaction mixture was stirred at room temperature overnight in the dark under a N₂ atmosphere. Evaporation of the MeCN solvent yielded a dark green residue, which was triturated with diethyl ether. The dark green solid was collected via vacuum filtration, washed with diethyl ether and pentane, and further dried under high vacuum. Yield: 120 mg (75%). UV–vis, λ, nm (ε, M⁻¹, cm⁻¹), MeCN: 691 (483), 356 (1657). Anal. Found: C, 48.08; H, 6.05; N, 7.15; calcd for C₂₄H₃₄Br₂N₃Pd·CH₃CN·C₄H₁₀O: C, 48.30; H, 6.35; N, 7.51. Complex N3CPd^{III}Br₂ (4a) was prepared using the same synthetic procedure, with N3CHPd^{II}(OAc)₂ instead of ^pMeN3CHPd^{II}(OAc)₂.

Preparation of [^pMeN3CPd^{IV}Br₂] (BF₄) (5). In a 20 mL vial equipped with a small magnetic stir bar, ^pMeN₃CPd^{III}Br₂ (22.9 mg, 0.0363 mmol) was dissolved in MeCN (1 mL) and stirred. To the stirring reaction mixture was added a solution of thianthrenyl (Thn^{•+})

tetrafluoroborate (14.3 mg, 0.0471 mmol) in MeCN (1 mL). The solution changed from a dark green to a ruby red color over 5–10 min, and the reaction mixture was stirred for an additional 15 min. The solution was then concentrated, and diethyl ether was added to induce precipitation of a ruby red solid. The filtrate was decanted, and the product was collected and dried under high vacuum. Yield: 14.9 mg (57%). $^1\text{H NMR}$ (300 MHz, CD_3CN), δ : 1.67 (br s, 9H, tBu), 1.84 (br s, 9H, tBu-CH), 2.36 (s, 3H, Ph-CH₃), 4.08 (d, $J = 16.5$ Hz, 2H, $-\text{CH}_2-$), 4.56 (d, $J = 18$ Hz, 2H, $-\text{CH}_2-$), 5.08 (d, $J = 16.5$ Hz, 2H, $-\text{CH}_2-$), 5.45 (d, $J = 18$ Hz, 2H, $-\text{CH}_2-$), 6.95 (s, 2H, Ph-H), 7.59 (d, 2H, Py-H_{meta}), 8.16 (t, 1H, Py-H_{para}). UV-vis, λ , nm (ϵ , M^{-1} , cm^{-1}), MeCN: 490 (1276), 327 (3907). Several attempts to obtain elemental analysis data proved unsuccessful, likely due to the decomposition of **5** during transportation and handling.

Preparation of $[\text{P}^{\text{Me}}\text{N}_3\text{CPd}^{\text{III}}(\text{MeCN})_2](\text{PF}_6)_2$ (6**).** *Method 1:* To a 20 mL vial equipped with a small magnetic stir bar was added a solution of $[\text{P}^{\text{Me}}\text{N}_3\text{CPd}^{\text{III}}\text{Br}_2]$ (49.8 mg, 0.079 mmol) in MeCN (1 mL). To the stirring dark green solution was added TlPF₆ (55.2 mg, 0.158 mmol) in MeCN (1 mL). An immediate color change to dark purple was observed. The mixture was stirred for 30 min and then filtered through a cotton plug. Subsequently, diethyl ether was added to the filtrate and the solution was cooled to -35 °C for 1 h. Diethyl ether solution was decanted, and a dark purple solid was collected and further dried under high vacuum. Yield: 40.0 mg (60%). *Method 2:* To a solution of $[\text{P}^{\text{Me}}\text{N}_3\text{CPd}^{\text{III}}(\text{Cl})(\text{MeCN})](\text{ClO}_4)$ (24.5 mg, 0.046 mmol) in MeCN was added a solution of TlPF₆ (16.1 mg, 0.046 mmol) in MeCN. The reaction mixture was stirred for 1 h, during which time the solution changed from a dark green to a purple color. After 1 h, the mixture was filtered and diethyl ether was added to the filtrate and the solution was cooled to -35 °C for 1 h. The diethyl ether solution was decanted, and the dark purple solid was collected and dried under high vacuum. Yield: 23.1 mg (60%). UV-vis, λ , nm (ϵ , M^{-1} , cm^{-1}), MeCN: 550 (1450), 344 (1519). Anal. Found: C, 41.81; H, 4.83; N, 8.55. Calculated for $\text{C}_{28}\text{H}_{40}\text{N}_5\text{PdClO}_4\text{PF}_6$: C, 42.17; H, 5.06; N, 8.78.

Preparation of $[\text{P}^{\text{Me}}\text{N}_3\text{CPd}^{\text{IV}}(\text{MeCN})_2](\text{PF}_6)_2(\text{BF}_4)$ (7**).** In a 20 mL vial equipped with a small magnetic stir bar, $[\text{P}^{\text{Me}}\text{N}_3\text{CPd}^{\text{III}}(\text{MeCN})_2](\text{PF}_6)_2$ (34.2 mg, 0.04 mmol) was dissolved in MeCN (2 mL) and stirred. To the stirring reaction mixture was added a solution of NOBF₄ (6.1 mg, 0.05 mmol) in MeCN (1 mL). The solution changed from purple to dark orange over 15 min, and the reaction mixture was stirred for an additional 15 min. Then the solvent was evaporated and the residue was triturated with pentane to give a dark orange powder, which was filtered and dried under high vacuum. Yield: 30.5 mg (82%). $^1\text{H NMR}$ (300 MHz, CD_3CN), δ : 1.66 (br s, 18H, N-tBu), 2.41 (s, 3H, p-CH₃-Ph), 4.41 (d, $J = 16.5$ Hz, 2H, $-\text{CH}_2-$), 4.91 (d, $J = 18$ Hz, 2H, $-\text{CH}_2-$), 5.20 (d, $J = 16.5$ Hz, 2H, $-\text{CH}_2-$), 5.48 (d, $J = 18$ Hz, 2H, $-\text{CH}_2-$), 7.10 (s, 2H, Ph-H), 7.75 (d, $J = 7.5$ Hz, 2H, Py-H_{meta}), 8.37 (t, $J = 7.5$ Hz, 1H, Py-H_{para}). Several attempts to obtain additional spectroscopic characterization and elemental analysis data for **7** proved unsuccessful, likely due to its limited stability.

General Procedure for X-ray Structure Determination. Crystals of X-ray diffraction quality were obtained by slow ether vapor diffusion into the corresponding acetonitrile or dichloromethane solution of **2a**, **2b**, **3**, **4a**, **4b**, and **6**. Suitable crystals of appropriate dimensions were mounted on Mitgen loops in random orientations. Preliminary examination and data collection were performed using a Bruker Kappa Apex-II Charge Coupled Device (CCD) Detector system single crystal X-ray diffractometer equipped with an Oxford Cryostream LT device. Data were collected using graphite monochromated Mo $K\alpha$ radiation ($\lambda = 0.71073$ Å) from a fine focus sealed tube X-ray source. Preliminary unit cell constants were determined with a set of 36 narrow frame scans. Typical data sets consist of a combination of ω and ϕ scan frames with a typical scan width of 0.5° and counting time of 15–30 s/frame at a crystal-to-detector distance of ~ 4.0 cm. The collected frames were integrated using an orientation matrix determined from the narrow frame scans. Apex II and SAINT software packages³⁰ were used for data collection and data integration. Analysis of the integrated data did not show any

decay. Final cell constants were determined by global refinement of reflections from the complete data set. Data were corrected for systematic errors using SADABS³⁰ based on the Laue symmetry using equivalent reflections.

Structure solutions and refinement were carried out using the SHELXTL-PLUS software package.³¹ The structures were refined with full-matrix least-squares refinement by minimizing $\sum w(F_o^2 - F_c^2)^2$. All non-hydrogen atoms were refined anisotropically to convergence. Typically, H atoms are added at the calculated positions in the final refinement cycles.

General Procedure for XPS Experiments. The XPS experiments were performed at the Washington University Institute of Materials Science and Engineering. Solid samples of $[\text{P}^{\text{Me}}\text{N}_3\text{CPd}^{\text{III}}\text{Br}_2]$ (**4b**) and $[\text{P}^{\text{Me}}\text{N}_3\text{CPd}^{\text{IV}}\text{Br}_2](\text{BF}_4)$ (**5**) were prepared and stored on dry ice prior to XPS analysis. Immediately prior to analysis, the two samples were transferred at RT to a piece of tape prefixed to the XPS plate. The samples were compressed and quickly loaded into the instrument. XPS spectra were recorded on a PHI 5000 Versa Probe II X-ray Photoelectron Spectrometer.

RESULTS AND DISCUSSION

Synthesis and Characterization of $\text{P}^{\text{R}}\text{N}_3\text{CHPd}^{\text{II}}(\text{OAc})_2$ Complexes. The $\text{N}_3\text{CHPd}^{\text{II}}(\text{OAc})_2$, **2a**, complex was synthesized by the reaction of N_3CH , **1a**, with 1 equiv of $\text{Pd}(\text{OAc})_2$ in CH_2Cl_2 . X-ray crystallography of **2a** reveals a square planar geometry around the Pd center with the pyridine N atom and one of the amine N atoms bound in addition to the two acetate ligands (Figure 1). Interestingly, the H15 atom

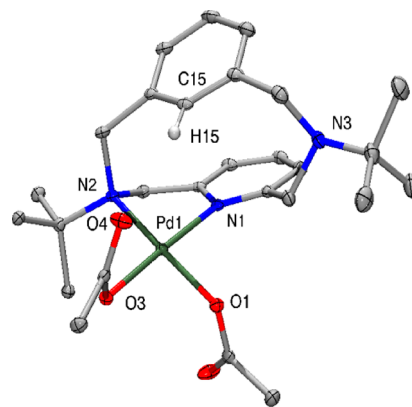


Figure 1. ORTEP representation (50% probability ellipsoids) of **2a**. Selected bond distances and angles: Pd1–N1 2.0144(19), Pd1–N2 2.0933(19), Pd1–O1 2.0179(16), Pd1–O3 2.0418(16), Pd1–H15 2.811, Pd1–C15 3.200, O4–H15 2.538, Pd1–H15–C15 105.6.

lies approximately 2.81 Å from the Pd center and 2.53 Å from O4, which faces toward the hydrogen atom and lies above the Pd center. This observation is indicative of a weak “anagostic” interaction between the C15–H15 bond and Pd, as well as a H-bond between H15 and O4.³² A similar $\text{Pd}\cdots\text{H}-\text{C}_{\text{ipso}}$ anagostic interaction was observed for a related $(\text{N}_3\text{CH})\text{-Ni}^{\text{II}}\text{Br}_2$ complex that was reported recently.^{23–26}

Further support for the presence of an anagostic interaction is obtained from the $^1\text{H NMR}$ of **2a**, which shows a downfield singlet corresponding to one proton at 11.1 ppm, in accord with the hydrogen-bonded nature of an anagostic interaction.³³ In addition, the eight pyridinophane methylene protons are inequivalent and thus appear as an AB (AX) pattern in the $^1\text{H NMR}$.³⁴ The *tert*-butyl groups on the amine atoms are also inequivalent since N2 is bound to the Pd center while N3 remains unbound. van Koten and co-workers have previously

observed similar behavior in an NCN pincer complex of the form $[\text{PdX}((^t\text{Bu})\text{MeNCN})]$.³⁵ In addition, the cyclic voltammogram (CV) of **2a** in 0.1 M $\text{Bu}_4\text{NClO}_4/\text{MeCN}$ shows two irreversible oxidation waves at 931 mV and 1125 mV vs Fc^+/Fc , tentatively assigned to $\text{Pd}^{\text{II/III}}$ and $\text{Pd}^{\text{III/IV}}$ redox couples, respectively (Figure 2). The relatively high oxidation

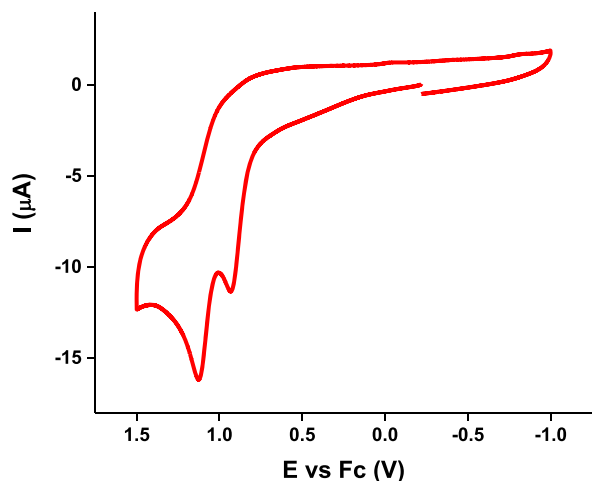


Figure 2. CV of $\text{N}_3\text{CHPd}^{\text{II}}(\text{OAc})_2$, **2a** (0.1 M $\text{Bu}_4\text{NClO}_4/\text{MeCN}$, 100 mV s^{-1} scan rate).

potentials can be attributed to a significant conformation change that needs to occur at the Pd center in order to stabilize the high-valent Pd species.^{11,36,37}

The close proximity of H13 to the Pd center suggests that the ligand can be tuned in order to promote the metal-mediated activation of the $\text{C}_{\text{ipso}}-\text{H}$ bond. Thus, we set out to probe whether employing phenyl donor groups with either electron-withdrawing or electron-donating *p*-substituents would increase the likelihood of $\text{C}_{\text{ipso}}-\text{H}$ bond activation and stabilization of a possible C–H activated Pd^{II} complex.^{38,39} In order to probe this possibility, we synthesized ligands possessing electron-donating groups (**1b**: R = Me, **1c**: R = OMe) and an electron-withdrawing group (**1d**: R = CN) in the *para* position relative to the $\text{C}_{\text{ipso}}-\text{H}$ bond.

The $^{\text{pMe}}\text{N}_3\text{CHPd}^{\text{II}}(\text{OAc})_2$ (**2b**) complex was synthesized via the reaction of $^{\text{pMe}}\text{N}_3\text{CH}$ (**1b**) with 1 equiv of $\text{Pd}(\text{OAc})_2$ in CH_2Cl_2 . X-ray crystallography of **2b** reveals similar metrical parameters to those **2a**, with the H13 atom approximately 2.81 Å from the Pd center and 3.18 Å from O2 (Figure 3). Interestingly, similar $\text{Pd}\cdots\text{H}_{\text{ipso}}$ distances to those observed in **2a** and **2b** were reported in the literature for Pd^{II} complexes having anagostic $\text{Pd}\cdots\text{H}$ interactions (Table 1).⁴⁰

Furthermore, ^1H NMR of **2b** shows a downfield singlet corresponding to one proton at 10.6 ppm. A $^1\text{J}_{\text{C-H}}$ coupling constant of 159 Hz was obtained via a modified HSQC experiment, which was carried out by turning off the ^{13}C decoupling during acquisition and allowed for the $^1\text{J}_{\text{CH}}$ coupling constant to be measured. On the basis of our previous assertion that H13 is interacting with the metal center in an anagostic manner, and thus the $^1\text{J}_{\text{C-H}}$ coupling constant should not be significantly affected, the measured value of 159 Hz is similar to typical arene $\text{C}_{\text{sp}^2}-\text{H}$ bonds.⁴¹ In addition, the CV of **2b** shows three irreversible oxidation waves at 514, 798, and 988 mV vs Fc^+/Fc , respectively, the first two likely corresponding to $\text{Pd}^{\text{II/III}}$ redox couples for two different ligand

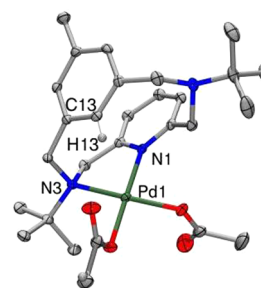


Figure 3. ORTEP representation (50% probability ellipsoids) of **2b**. Selected bond distances and angles: Pd1–N1 2.0188(15), Pd1–N3 2.1113(15), Pd1–O1 2.0166(13), Pd1–O3 2.0288(13), Pd1–H13 2.808, Pd1–C13 3.180, O2–H13 3.180, Pd1–H13–C13 104.4.

Table 1. Comparison of Pd– H_{ipso} Bond Distances and Angles for Pd^{II} Complexes

Pd^{II} Complex	M–H distance (Å)	C–H–M angle (deg)
2a	2.81	105.6
2b	2.81	104.4
DAGGUN ^a	2.95	112.8
DUHYUA ^a	2.78	102.1
DUNWAK ^a	2.94	99.8
EFODEI ^a	2.88	107.5
HAPNIV ^a	2.93	115.3

^aPreviously reported complexes are identified by their CCDC reference code.⁴⁰

conformations,^{11,36,37} while the third corresponds to a $\text{Pd}^{\text{III/IV}}$ redox couple (Figure 4).

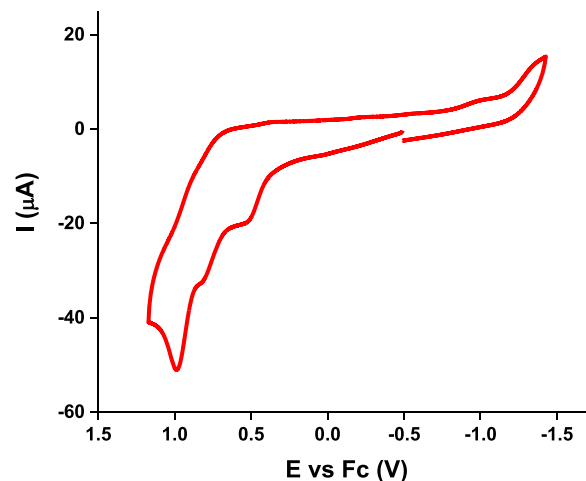


Figure 4. CV of $^{\text{pMe}}\text{N}_3\text{CHPd}^{\text{II}}(\text{OAc})_2$, **2b** (0.1 M $\text{Bu}_4\text{NClO}_4/\text{MeCN}$, 100 mV s^{-1} scan rate).

Reaction of $^{\text{pOMe}}\text{N}_3\text{CH}$ (**1c**) and $^{\text{pCN}}\text{N}_3\text{CH}$ (**1d**) with 1 equiv of $\text{Pd}(\text{OAc})_2$ in CH_2Cl_2 produced complexes **2c** and **2d** in 70% and 75% isolated yields, respectively (Scheme 1). ^1H NMR of **2c** and **2d** reveal downfield singlets at 10.4 and 11.4 ppm, respectively (Table 2). These peaks likely correspond to a $\text{C}_{\text{sp}^2}-\text{H}$ proton weakly interacting with the Pd center, analogous to H15 in **2a** and H13 in **2b**.

Interestingly, $\text{C}_{\text{ipso}}-\text{H}$ activation is not observed upon heating or addition of excess acetate to solutions of **2b–d** in MeCN, only decomposition to Pd black being observed in each case. The lack of C–H bond activation in these Pd^{II}

Table 2. Comparison of H_{ipso} ^1H Chemical Shifts for Pd Complexes and Arene Analogues

Pd ^{II} complex	H_{ipso} ^1H NMR shift (ppm)	arene analogue	H_{ipso} ^1H NMR shift (ppm)
2a	10.90	xylene	6.96
2b	10.64	mesitylene	6.96
2c	10.47	3,5-dimethylanisole	6.99
2d	11.41	3,5-dimethylbenzonitrile	7.24

precursors could be due to the rigid nature of the macrocyclic $^{\text{R}}\text{N}_3\text{CH}$ ligand that does not allow for a close $\text{Pd}\cdots\text{H}-\text{C}$ interaction and only supports a weak anagostic interaction; moreover, the $\text{C}_{\text{ipso}}-\text{H}$ bond is not positioned in the equatorial plane of the square planar Pd^{II} center, which is usually required for a concerted metalation-deprotonation type of C–H bond activation.^{12–16} These geometric considerations suggest that the activation of the $\text{C}_{\text{ipso}}-\text{H}$ bond by Pd cannot be induced by simply altering the electron density on the bond. However, the observation of a downfield chemical shift signal in **2a–d** suggests a significant deshielding effect of the Pd center on the *ipso*-H in the corresponding complexes (10.4–11.4 ppm, Table 2). For comparison, xylene and its analogues mesitylene,³⁹ 3,5-dimethylanisole,⁵ and 3,5-dimethylbenzonitrile⁴² show a smaller variance (6.96–7.24 ppm) in the ^1H NMR chemical shifts of the *para*-H atoms.

Synthesis and X-ray Crystallography of $^{\text{R}}\text{N}_3\text{CPd}^{\text{III}}\text{X}_2$ Complexes. Interestingly, when **2b** was treated with 1 equiv of PhICl_2 , a well-known two-electron oxidant,⁴³ the stable Pd^{III} complex $[\text{P}^{\text{Me}}\text{N}_3\text{CPd}^{\text{III}}(\text{Cl})(\text{MeCN})](\text{ClO}_4)$, **3**, was obtained upon addition of LiClO_4 . While the mechanism of this reaction is not completely understood, one possibility might involve the formation of a transient Pd^{IV} intermediate, followed by a comproportionation reaction between this species and the starting Pd^{II} complex **2b**, although a direct one-electron oxidation pathway cannot be excluded since PhICl_2 could also act as a one-electron oxidant.⁴⁴ X-ray crystallography of **3** reveals that the Pd^{III} center adopts a distorted octahedral geometry, with one chloride anion and one MeCN ligand bound equatorially to the Pd center (Scheme 1 and Figure 5).

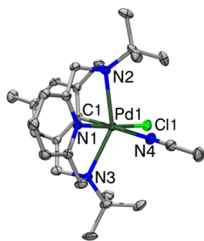


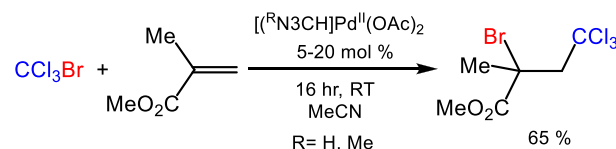
Figure 5. ORTEP representation (50% probability ellipsoids) of **3**. Selected bond distances and angles: Pd1–C1 1.945(3), Pd1–N1 2.043(2), Pd1–N4 2.180(2), Pd1–Cl1 2.3568(8), Pd1–N3 2.375(2), Pd1–N2 2.391(2), N3–Pd1–N2 147.03(8).

The chloride ligand is bound *trans* to the pyridyl N atom, while the more weakly interacting MeCN ligand is bound *trans* to the phenyl C atom, as expected due the significant *trans* influence of the phenyl group.^{45,46} Importantly, since in **3** the $\text{C}_{\text{ipso}}-\text{H}$ bond has been activated upon oxidation and a Pd^{III}–C bond has been formed, we propose that C–H bond activation has been promoted by the oxidation of **2b** and thus has likely occurred at a Pd^{III} (or Pd^{IV}) center, in a similar

manner to what we observed recently for analogous Ni complexes.^{23–26}

Pd^{II} Complexes are known catalysts for the Kharasch radical addition of polyhaloalkanes to alkenes.^{47–50} Therefore, we probed the reaction of methyl methacrylate and bromotrichloromethane (CCl_3Br) with **2a** and **2b** acting as Pd^{II} catalysts, to give good yields of the addition product at RT overnight (Scheme 2). Interestingly, the reaction mixture turns

Scheme 2. Kharasch Radical Addition Catalyzed by $^{\text{P}^{\text{Me}}}\text{N}_3\text{CHPd}^{\text{II}}(\text{OAc})_2$



dark green within minutes due to the formation of Pd^{III} complexes identified as $^{\text{R}}\text{N}_3\text{CPd}^{\text{III}}\text{Br}_2$ (**4a**: R = H, **4b**: R = Me), which can be isolated from the reaction mixture as stable dark green solids. X-ray crystallography of **4a** and **4b** reveals the presence of a distorted octahedral environment around the Pd^{III} center with two bromide anions bound equatorially (Figures 6 and 7). In addition, the $\text{C}_{\text{ipso}}-\text{H}$ bond of the phenyl

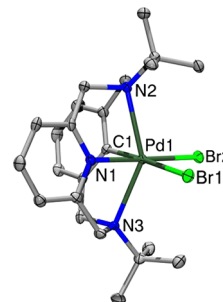


Figure 6. ORTEP representation (50% probability ellipsoids) of **4a**. Selected bond distances and angles: Pd1–Br1 2.5993(4), Pd1–Br2 2.4869(4), Pd1–N1 2.034(3), Pd1–C1 1.974(4), Pd1–N2 2.442(3), Pd1–N3 2.446(3), N3–Pd1–N2 145.6(5).

groups has been activated during the catalytic process, which further supports our previous assertion that the C–H activation in **2a** and **2b** occurs upon the oxidation of the Pd^{II} center to Pd^{III} (or Pd^{IV}). A possible mechanism for

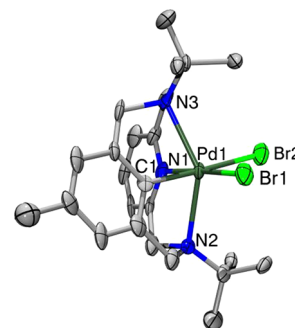


Figure 7. ORTEP representation (30% probability ellipsoids) of **4b**. Selected bond distances and angles: Pd1–Br1 2.499(3), Pd1–Br2 2.518(3), Pd1–N1 2.028(16), Pd1–C1 1.989(17), Pd1–N2 2.431(13), Pd1–N3 2.422(13), N3–Pd1–N2 145.6(5).

reaction of **2a/2b** with CCl_3Br and MMA involves a reversible electron transfer/halogen transfer from bromotrichloromethane to the Pd center, which leads to the oxidation of Pd^{II} and Pd^{III} and formation of CCl_3 radicals.^{47–50} Addition of the CCl_3 radical to MMA, followed by halogen transfer from Pd^{III} , should generate the addition product and regenerate **2a/2b**. However, during the catalytic process, the $\text{C}_{\text{ipso}}\text{–H}$ bond activation is likely to occur at Pd^{III} (or Pd^{IV}), and the resulting organometallic complex is further stabilized by binding a second bromide ligand to generate **4a/4b**.⁵¹

We further probed the chemistry of **4b** with TlPF_6 , a well-known halide abstraction reagent. Reaction of **4b** with 1 equiv of TlPF_6 resulted in the isolation of a purple complex identified as $[\text{p}^{\text{Me}}\text{N}_3\text{CPd}^{\text{III}}(\text{MeCN})_2](\text{PF}_6)_2$, **6**. Single crystal X-ray crystallography confirms the structure and connectivity of **6**, with the complex adopting a distorted octahedral geometry around the Pd center and two acetonitrile ligands bound equatorially around the Pd center (Figure 8), and similar to the analogous Ni(III)-bis-solvento complexes reported recently.^{23–26}

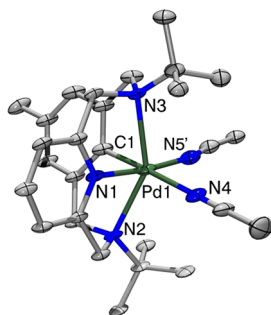


Figure 8. ORTEP representation (30% probability ellipsoids) of **6**. Selected bond distances and angles: Pd1–C1 1.958(14), Pd1–N1 2.009(11), Pd1–N4 2.162(12), Pd1–N5' 2.07(2), Pd1–N2 2.365(10), Pd1–N3 2.390(10), N3–Pd1–N2 147.7(4).

Spectroscopic Properties of $[\text{p}^{\text{R}}\text{N}_3\text{CPd}^{\text{III}}\text{X}_2]$ Complexes. The EPR spectra of **3**, **4b**, and **6** display rhombic, anisotropic signals characteristic of a Pd^{III} , d^7 center with a d_z^2 ground state (Figure 9), while the EPR spectrum of **6** exhibits a pattern that has been observed for $(\text{R}^{\text{N}}\text{3C})\text{Ni}^{\text{III}}$ bis-solvento complexes.^{23–26} Furthermore, the CV of **3** reveals a quasi-reversible $\text{Pd}^{\text{III/IV}}$ redox couple at 452 mV vs Fc and an irreversible $\text{Pd}^{\text{III/II}}$ reduction peak at -518 mV vs Fc (Figure 10 and Table 3). Interestingly, the $\text{Pd}^{\text{III/IV}}$ redox couple is lower for **4b** at 283 mV vs Fc (Figure 10), whereas, for **6**, the $\text{Pd}^{\text{III/IV}}$ oxidation potential is higher at 650 mV (vs Fc). The observed trend indicates that the $\text{Pd}^{\text{III/IV}}$ oxidation potential increases with increasing electrophilicity of the metal center, with **4b** containing a neutral Pd^{III} center while **6** contains a dicationic Pd^{III} center. The relatively low $\text{Pd}^{\text{III/IV}}$ oxidation potential for **4b** and **3** indicates that mild oxidants can be used to access the Pd^{IV} oxidation state, while stronger oxidants are needed for **6**. However, the ability to access Pd^{IV} from either **3**, **4b**, or **6** could allow us to study the reactivity of the $\text{p}^{\text{Me}}\text{N}_3\text{CPd}$ system with a wide variety of organic substrates that could bind via transmetalation reactions or in the “open” coordination sites occupied by the labile acetonitrile ligands. Also, the same trends observed above for the electrochemical properties of the Pd^{III} complexes are likely responsible for observed blue shift in the UV–vis spectra from **4b** to **6** (Figure 11 and Table 3).

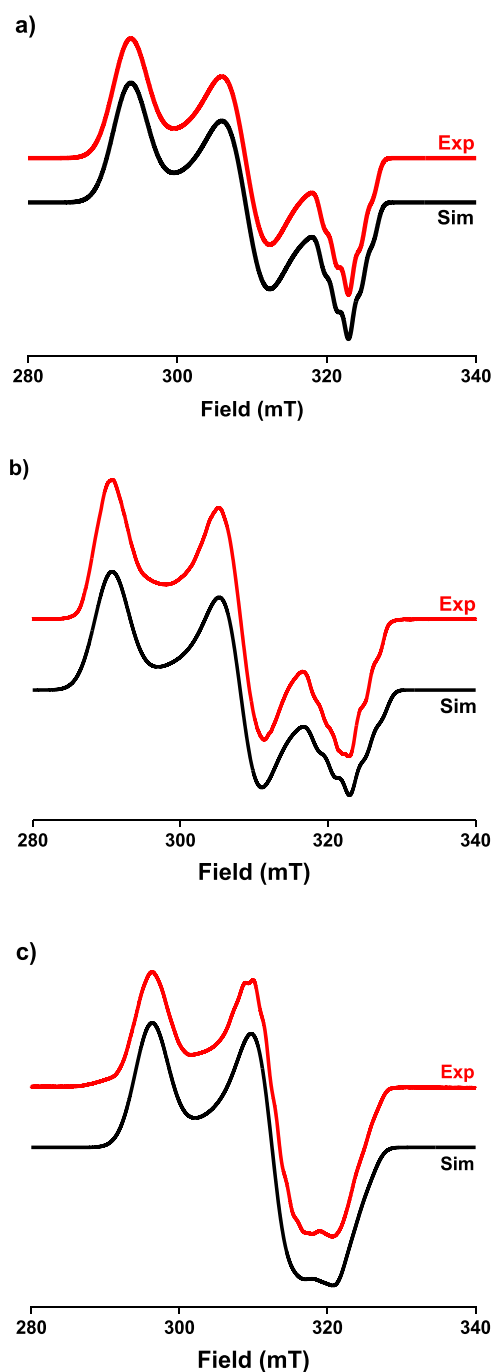


Figure 9. EPR spectra (in 1:3 MeCN:PrCN glass, 77 K) of (a) **3**, (b) **4b**, and (c) **6**. Simulation parameters are listed in Table 3.

Synthesis and Characterization of $[\text{p}^{\text{Me}}\text{N}_3\text{CPd}^{\text{IV}}]$ Complexes. Further chemical oxidation of **4b** with 1 equiv of thianthrenyl tetrafluoroborate ($\text{Thn}^{\bullet+}$) BF_4 yields the Pd^{IV} complex $[\text{p}^{\text{Me}}\text{N}_3\text{CPd}^{\text{IV}}\text{Br}_2](\text{BF}_4)$, **5**, as a ruby red solid (Scheme 3). The identity of the diamagnetic, d^6 complex **5** was confirmed by ^1H NMR spectroscopy and UV–vis spectroscopy. Further evidence for the successful oxidation of **4b** to **5** was gained using X-ray photoelectron spectroscopy (XPS), which shows an increase in the Pd $2_{p3/2}$ and $2_{p1/2}$ binding energies of 3 eV between **4b** and **5**, and thus strongly suggests the presence of a more oxidized Pd center in **5** vs the Pd^{III} complex **4b** (Figure 12). The XPS data also indicate that the solid isolated from the reaction mixture contains ~60% of

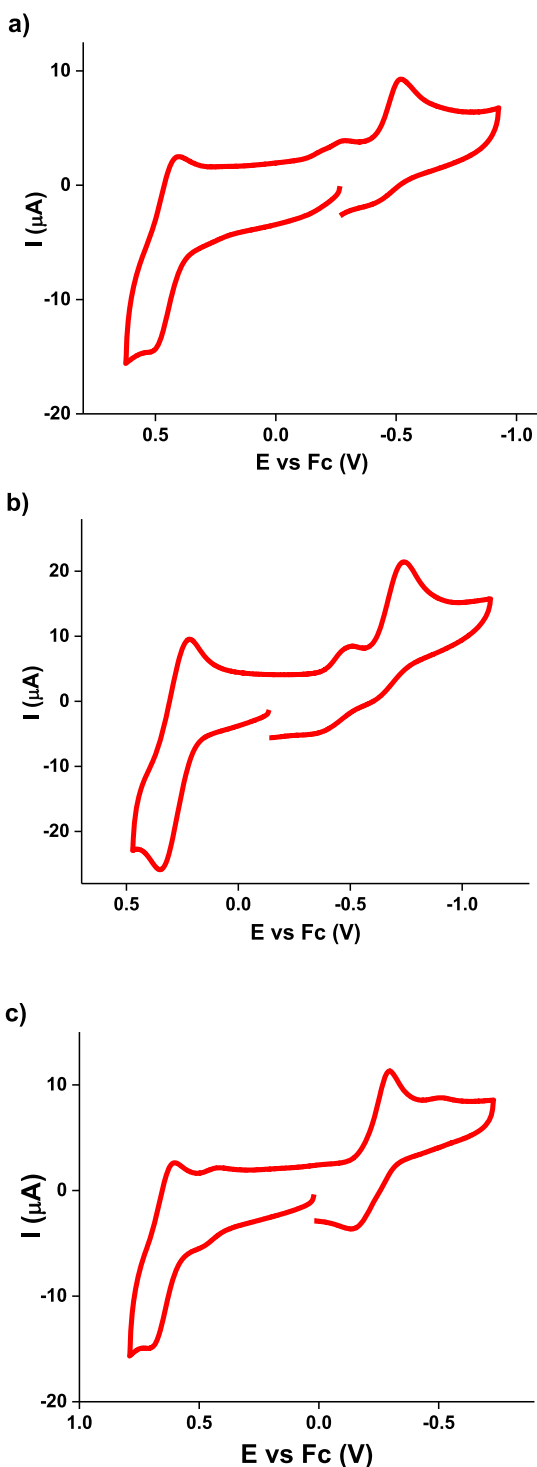


Figure 10. Cyclic voltammograms of (a) 3, (b) 4b, and (c) 6 (0.1 M $\text{Bu}_4\text{NClO}_4/\text{MeCN}$, 100 mV s^{-1} scan rate).

the Pd^{IV} species 5 and $\sim 40\%$ of a Pd^{III} species, which is likely due to reduction of the Pd^{IV} species in the reaction solution or during the setup of the XPS experiment.

Finally, we were pleased to observe that oxidation of the $[\text{p}^{\text{Me}}\text{N}_3\text{CPd}^{\text{III}}(\text{MeCN})_2](\text{PF}_6)_2$ complex 6 with 1 equiv of NOBF_4 yields the tricationic Pd^{IV} complex $[\text{p}^{\text{Me}}\text{N}_3\text{CPd}^{\text{IV}}(\text{MeCN})_2](\text{PF}_6)_2(\text{BF}_4)$, 7, as a dark orange solid (Scheme 3), which was characterized by ^1H NMR spectroscopy. While complex 7 exhibits limited stability, it is important to note that

Table 3. Electrochemical and Spectroscopic Properties of Pd^{III} Complexes

complex	$E_{1/2}^{\text{III/IV}}$, $E_{\text{pc}}^{\text{III/II}}$ (mV) ^a	UV-vis, λ , nm (ϵ , $\text{M}^{-1}\text{cm}^{-1}$) ^b	EPR, g_x , g_y , g_z (A_{2N} , G) ^c
3	452 (100), -288/-518	638 (551), 473 (548), 355 (1565)	2.236, 2.109, 2.013 (18.0)
4b	283 (134), -497/-740	691 (483), 356 (1657)	2.213, 2.102, 2.013 (16.0)
6	650 (96), -298	550 (1450), 344 (2322)	2.193, 2.079, 2.022 (21.0)

^aPotentials in CV measurements are against Fc^+/Fc in 0.1 M $\text{Bu}_4\text{NClO}_4/\text{MeCN}$, scan rate 100 mV/s ; ΔE_p is the peak potential separation for the $\text{Pd}^{\text{III}}/\text{Pd}^{\text{IV}}$ couple. ^bUV-vis spectra collected in MeCN at RT. ^cEPR spectra collected in 1:3 MeCN:PrCN glasses at 77 K; superhyperfine coupling constants between the two axial amine donors and the Pd^{III} center.

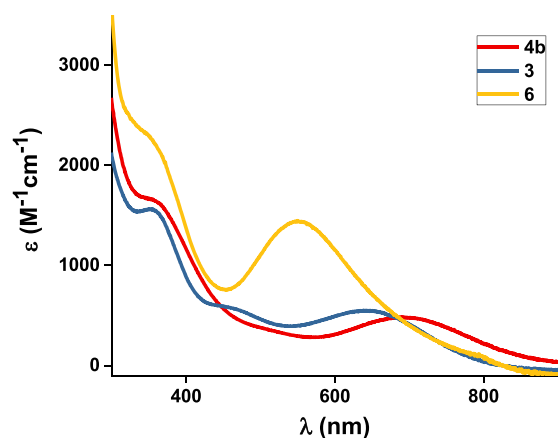
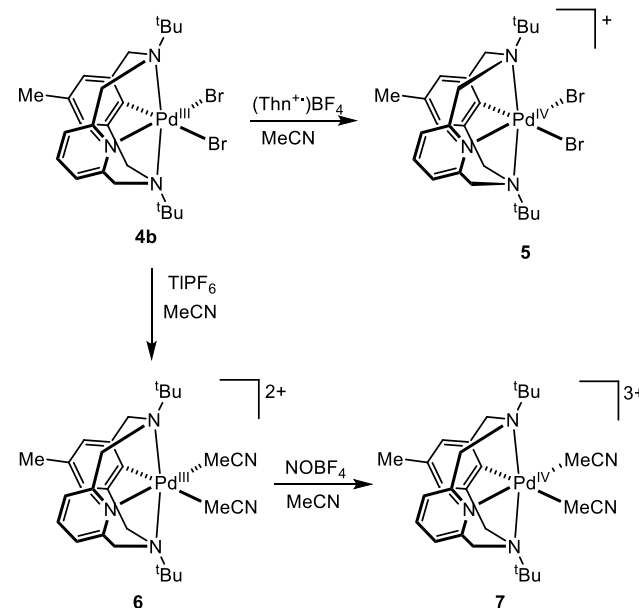


Figure 11. Overlay of UV-vis spectra for 3, 4b, and 6 in MeCN at RT.

Scheme 3. Synthesis of $\text{p}^{\text{Me}}\text{N}_3\text{CPd}^{\text{IV}}\text{X}_2$ ($\text{X} = \text{Br}, \text{MeCN}$) Complexes



this is to the best of our knowledge the first tricationic, organometallic Pd^{IV} complex reported to date,⁵² and is thus expected to exhibit an increased electrophilic character that

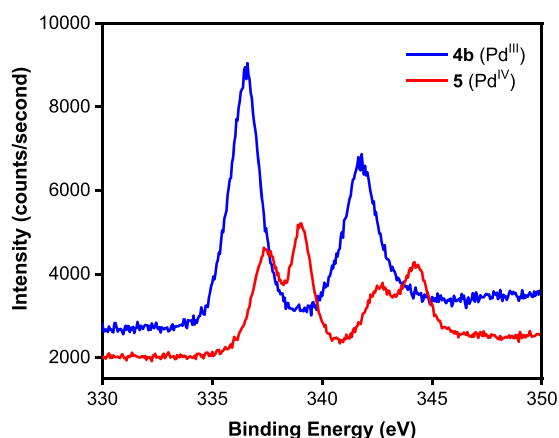


Figure 12. XPS spectral comparison of ${}^{\text{PMe}}\text{N}_3\text{CPd}^{\text{III}}\text{Br}_2$ (**4b**) and $[\text{PMe}\text{N}_3\text{CPd}^{\text{IV}}\text{Br}_2](\text{BF}_4)$ (**5**).

could help promote facile C–C and C–heteroatom bond formation reactions.^{12–16}

Overall, these results show that use of the ${}^{\text{R}}\text{N}_3\text{CH}$ ligands allows the formation of Pd^{III} - and Pd^{IV} -halide complexes in which the *ispo*-C–H bond of the ligand has been activated. With these Pd-halide complexes in hand, we are currently performing detailed transmetalation reactivity studies and subsequent C–C and C–heteroatom bond formation transformations at both Pd^{III} and Pd^{IV} centers.

CONCLUSION

In conclusion, we have successfully isolated and characterized a series of Pd^{II} , Pd^{III} , and Pd^{IV} complexes stabilized by the tetradentate ligand ${}^{\text{R}}\text{N}_3\text{CH}$. The structure of this ligand system allowed us to probe the possibility of intramolecular C–H activation at the Pd center. Interestingly, in the isolated Pd^{II} complexes ${}^{\text{R}}\text{N}_3\text{CHPd}^{\text{II}}(\text{OAc})_2$ (**2a–d**), an anagostic interaction is observed between one of the C–H bonds and the Pd center. Addition of excess acetate or heat fails to induce the activation of this C–H bond at the Pd^{II} oxidation state. This observation indicates that the ${}^{\text{R}}\text{N}_3\text{CHPd}^{\text{II}}(\text{OAc})_2$ complexes are held in a rigid conformation that does not allow for a close $\text{Pd}\cdots\text{H}-\text{C}$ interaction and only supports a weak anagostic interaction. Only upon oxidation to a Pd^{III} complex with PhICl_2 or CCl_3Br is C–H activation observed, thus suggesting that the complexes discussed above exhibit the propensity for facile oxidatively-induced reactivity. Current efforts aimed at further probing the reactivity of these systems and elucidating the mechanism of the oxidation reactions are underway.

ASSOCIATED CONTENT

Supporting Information

The Supporting Information is available free of charge on the ACS Publications website at DOI: 10.1021/acs.organomet.9b00505.

¹H NMR spectra of **1a,b**, **2a–d**, and **5**; spectroscopic characterization; X-ray crystallographic data (PDF)

Accession Codes

CCDC 1586734–1586739 contain the supplementary crystallographic data for this paper. These data can be obtained free of charge via www.ccdc.cam.ac.uk/data_request/cif, or by emailing data_request@ccdc.cam.ac.uk, or by contacting The Cambridge Crystallographic Data Centre, 12 Union Road, Cambridge CB2 1EZ, UK; fax: +44 1223 336033.

AUTHOR INFORMATION

Corresponding Author

*E-mail: mirica@illinois.edu.

ORCID

Julia R. Khusnutdinova: 0000-0002-5911-4382

Liviu M. Mirica: 0000-0003-0584-9508

Notes

The authors declare no competing financial interest.

ACKNOWLEDGMENTS

We thank the Department of Energy's BES Catalysis Science Program (DE-SC0006862) for financial support. We would also like to thank Dr. Brian Marsden and Dr. Jeff Kao at the WU High Resolution NMR facility for assistance with the characterization of the ${}^{\text{PR}}\text{N}_3\text{CHPd}^{\text{II}}(\text{OAc})_2$ complexes, and Dr. Jason Schultz for his assistance with the EPR and XPS experiments.

REFERENCES

- (1) Negishi, E. *Handbook of Organopalladium Chemistry for Organic Synthesis*; John Wiley & Sons: Hoboken, NJ, 2002; p 3424.
- (2) Hartwig, J. F. *Organotransition Metal Chemistry: From Bonding to Catalysis*; University Science Books: Sausalito, CA, 2010; p 1127.
- (3) Lyons, T. W.; Sanford, M. S. Palladium-Catalyzed Ligand-Directed C-H Functionalization Reactions. *Chem. Rev.* **2010**, *110* (2), 1147–1169.
- (4) Muñiz, K. High-Oxidation-State Palladium Catalysis: New Reactivity for Organic Synthesis. *Angew. Chem., Int. Ed.* **2009**, *48* (50), 9412–9423.
- (5) Canty, A. J. Organopalladium and platinum chemistry in oxidising milieu as models for organic synthesis involving the higher oxidation states of palladium. *J. Chem. Soc., Dalton Trans.* **2009**, No. 47, 10409–10417.
- (6) Chen, X.; Engle, K. M.; Wang, D. H.; Yu, J. Q. Palladium(II)-Catalyzed C-H Activation/C-C Cross-Coupling Reactions: Versatility and Practicality. *Angew. Chem., Int. Ed.* **2009**, *48* (28), 5094–5115.
- (7) Sehnal, P.; Taylor, R. J. K.; Fairlamb, I. J. S. Emergence of Palladium(IV) Chemistry in Synthesis and Catalysis. *Chem. Rev.* **2010**, *110* (2), 824–889.
- (8) Desai, L. V.; Hull, K. L.; Sanford, M. S. Palladium-catalyzed oxygenation of unactivated sp³ C-H bonds. *J. Am. Chem. Soc.* **2004**, *126* (31), 9542–9543.
- (9) Xu, L.-M.; Li, B.-J.; Yang, Z.; Shi, Z.-J. Organopalladium(IV) chemistry. *Chem. Soc. Rev.* **2010**, *39* (2), 712–733.
- (10) Powers, D. C.; Ritter, T. Palladium(III) in Synthesis and Catalysis. *Top. Organomet. Chem.* **2011**, *35*, 129–156.
- (11) Khusnutdinova, J. R.; Rath, N. P.; Mirica, L. M. Stable Mononuclear Organometallic Pd(III) Complexes and Their C-C Bond Formation Reactivity. *J. Am. Chem. Soc.* **2010**, *132* (21), 7303–7305.
- (12) Powers, D. C.; Lee, E.; Ariafard, A.; Sanford, M. S.; Yates, B. F.; Canty, A. J.; Ritter, T. Connecting Binuclear Pd(III) and Mononuclear Pd(IV) Chemistry by Pd-Pd Bond Cleavage. *J. Am. Chem. Soc.* **2012**, *134* (29), 12002–12009.
- (13) Engle, K. M.; Mei, T.-S.; Wasa, M.; Yu, J.-Q. Weak Coordination as a Powerful Means for Developing Broadly Useful C-H Functionalization Reactions. *Acc. Chem. Res.* **2012**, *45* (6), 788–802.
- (14) Kalyani, D.; Dick, A. R.; Anani, W. Q.; Sanford, M. S. Scope and selectivity in palladium-catalyzed directed C-H bond halogenation reactions. *Tetrahedron* **2006**, *62* (49), 11483–11498.
- (15) Racowski, J. M.; Sanford, M. S. Carbon–Heteroatom Bond-Forming Reductive Elimination from Palladium(IV) Complexes. *Top. Organomet. Chem.* **2011**, *35*, 61–84.
- (16) Canty, A. J. Development of organopalladium(IV) chemistry: fundamental aspects and systems for studies of mechanism in

organometallic chemistry and catalysis. *Acc. Chem. Res.* **1992**, *25* (2), 83–90.

(17) Racowski, J. M.; Ball, N. D.; Sanford, M. S. C-H Bond Activation at Palladium(IV) Centers. *J. Am. Chem. Soc.* **2011**, *133* (45), 18022–18025.

(18) Maleckis, A.; Kampf, J. W.; Sanford, M. S. A Detailed Study of Acetate-Assisted C–H Activation at Palladium(IV) Centers. *J. Am. Chem. Soc.* **2013**, *135* (17), 6618–6625.

(19) Niu, J.-L.; Hao, X.-Q.; Gong, J.-F.; Song, M.-P. Symmetrical and unsymmetrical pincer complexes with group 10 metals: synthesis via aryl C–H activation and some catalytic applications. *Dalton Trans.* **2011**, *40* (19), 5135–5150.

(20) Bugarin, A.; Connell, B. T. A highly active and selective palladium pincer catalyst for the formation of alpha-aryl ketones via cross-coupling. *Chem. Commun.* **2011**, *47* (25), 7218–7220.

(21) Khusnutdinova, J. R.; Rath, N. P.; Mirica, L. M. The Aerobic Oxidation of a Pd(II) Dimethyl Complex Leads to Selective Ethane Elimination from a Pd(III) Intermediate. *J. Am. Chem. Soc.* **2012**, *134*, 2414–2422.

(22) Tang, F.; Zhang, Y.; Rath, N. P.; Mirica, L. M. Detection of Pd(III) and Pd(IV) Intermediates during the Aerobic Oxidative C–C Bond Formation from a Pd(II) Dimethyl Complex. *Organometallics* **2012**, *31* (18), 6690–6696.

(23) Zhou, W.; Schultz, J. W.; Rath, N. P.; Mirica, L. M. Aromatic Methoxylation and Hydroxylation by Organometallic High-Valent Nickel Complexes. *J. Am. Chem. Soc.* **2015**, *137* (24), 7604–7607.

(24) Zhou, W.; Rath, N. P.; Mirica, L. M. Oxidatively-induced aromatic cyanation mediated by Ni(III). *Dalton Trans.* **2016**, *45*, 8693–8695.

(25) Zhou, W.; Zheng, S. A.; Schultz, J. W.; Rath, N. P.; Mirica, L. M. Aromatic Cyanoalkylation through Double C–H Activation Mediated by Ni(III). *J. Am. Chem. Soc.* **2016**, *138* (18), 5777–5780.

(26) Zhou, W.; Watson, M. B.; Zheng, S.; Rath, N. P.; Mirica, L. M. Ligand effects on the properties of Ni(III) complexes: aerobically-induced aromatic cyanation at room temperature. *Dalton Trans.* **2016**, *45* (40), 15886–15893.

(27) Evans, D. F. The determination of the paramagnetic susceptibility of substances in solution by nuclear magnetic resonance. *J. Chem. Soc.* **1959**, 2003–5.

(28) Bain, G. A.; Berry, J. F. Diamagnetic Corrections and Pascal's Constants. *J. Chem. Educ.* **2008**, *85* (4), 532–536.

(29) Gemel, C.; Foltz, K.; Caulton, K. G. New Approach to Ru(II) Pincer Ligand Chemistry. Bis(tert-butylaminomethyl)pyridine Coordinated to Ruthenium(II). *Inorg. Chem.* **2000**, *39* (7), 1593–1597.

(30) *Apex II and SAINT*; Bruker Analytical X-Ray: Madison, WI, 2008.

(31) Sheldrick, G. A short history of SHELX. *Acta Crystallogr., Sect. A: Found. Crystallogr.* **2008**, *64* (1), 112–122.

(32) Braga, D.; Grepioni, F.; Tedesco, E.; Biradha, K.; Desiraju, G. R. Hydrogen Bonding in Organometallic Crystals. 6. X–H–M Hydrogen Bonds and M–(H–X) Pseudo-Agostic Bonds. *Organometallics* **1997**, *16* (9), 1846–1856.

(33) Brookhart, M.; Green, M. L. H.; Parkin, G. Agostic interactions in transition metal compounds. *Proc. Natl. Acad. Sci. U. S. A.* **2007**, *104* (17), 6908–6914.

(34) See the [Supporting Information](#).

(35) van Beek, J. A. M.; van Koten, G.; Dekker, G. P. C. M.; Wissing, E.; Zoutberg, M. C.; Stam, C. H. Synthesis and reactivity towards diiodine of palladium(II) and platinum(II) complexes with non-cyclic and cyclic ligands (C₆H₃{CH₂NR¹R²}}_{2,2,6})⁻. End-on diiodine-platinum(II) bonding in macrocyclic [Pt(C₆H₃{CH₂NMe(CH₂)-7MeNCH₂}}_{2,6})(η¹-I₂)]. *J. Organomet. Chem.* **1990**, *394* (1), 659–678.

(36) Tang, F. Z.; Qu, F. R.; Khusnutdinova, J. R.; Rath, N. P.; Mirica, L. M. Structural and reactivity comparison of analogous organometallic Pd(III) and Pd(IV) complexes. *Dalton Trans.* **2012**, *41* (46), 14046–14050.

(37) Khusnutdinova, J. R.; Rath, N. P.; Mirica, L. M. The Conformational Flexibility of the Tetradentate Ligand ^tBu₄N⁺ is

Essential for the Stabilization of (^tBu₄N⁺)Pd^{III} Complexes. *Inorg. Chem.* **2014**, *53*, 13112–13129.

(38) Bugarin, A.; Connell, B. T. Chiral Nickel(II) and Palladium(II) NCN-Pincer Complexes Based on Substituted Benzene: Synthesis, Structure, and Lewis Acidity. *Organometallics* **2008**, *27* (17), 4357–4369.

(39) Chow, W. K.; So, C. M.; Lau, C. P.; Kwong, F. Y. Palladium-catalyzed reductive cleavage of tosylated arenes using isopropanol as the mild reducing agent. *Org. Chem. Front.* **2014**, *1* (5), 464–467.

(40) Mukhopadhyay, A.; Pal, S. Intramolecular Apical C–H···M Interactions in Square-Planar Nickel(II) Complexes with Dianionic Tridentate Ligands and 2-Phenylimidazole. *Eur. J. Inorg. Chem.* **2006**, *2006* (23), 4879–4887.

(41) Pavia, D. L.; Lampman, G. M.; Kriz, G. S.; Vyvyan, J. A. *Introduction to Spectroscopy*, 4th ed.; Brooks/Cole, Cengage Learning: Belmont, CA, 2009.

(42) Shu, Z.; Ye, Y.; Deng, Y.; Zhang, Y.; Wang, J. Palladium(II)-Catalyzed Direct Conversion of Methyl Arenes into Aromatic Nitriles. *Angew. Chem., Int. Ed.* **2013**, *52* (40), 10573–10576.

(43) Powers, D. C.; Ritter, T. Bimetallic Pd(III) complexes in palladium-catalyzed carbon-heteroatom bond formation. *Nat. Chem.* **2009**, *1* (4), 302–309.

(44) Dröse, P.; Crozier, A. R.; Lashkari, S.; Gottfriedsen, J.; Blaurock, S.; Hrib, C. G.; Maichle-Mössmer, C.; Schädle, C.; Anwender, R.; Edelmann, F. T. Facile Access to Tetravalent Cerium Compounds: One-Electron Oxidation Using Iodine(III) Reagents. *J. Am. Chem. Soc.* **2010**, *132* (40), 14046–14047.

(45) Anderson, K. M.; Orpen, A. G. On the relative magnitudes of cis and trans influences in metal complexes. *Chem. Commun.* **2001**, No. 24, 2682–2683.

(46) Atwood, J. D. *Inorganic and Organometallic Reaction Mechanisms*; Brooks/Cole: Monterey, CA, 1985.

(47) Tsuji, J.; Sato, K.; Nagashima, H. Palladium-catalyzed addition reaction of polyhaloalkanes to olefins. *Tetrahedron* **1985**, *41* (2), 393–7.

(48) Gossage, R. A.; van de Kuil, L. A.; van Koten, G. Diaminoarylnickel(II) “Pincer” complexes: mechanistic considerations in the kharasch addition reaction, controlled polymerization, and dendrimeric transition metal catalysts. *Acc. Chem. Res.* **1998**, *31* (7), 423–431.

(49) van de Kuil, L. A.; Grove, D. M.; Gossage, R. A.; Zwikker, J. W.; Jenneskens, L. W.; Drenth, W.; van Koten, G. Mechanistic aspects of the Kharasch addition reaction catalyzed by organonickel(II) complexes containing the monoanionic terdentate arlydiamine ligand system [C₆H₂(CH₂NMe₂)₂-2,6-R-4]. *Organometallics* **1997**, *16* (23), 4985–4994.

(50) Motoda, D.; Kinoshita, H.; Shinokubo, H.; Oshima, K. A room temperature Kharasch reaction catalyzed by Pd(0) in a heterogeneous aqueous system. *Adv. Synth. Catal.* **2002**, *344* (3–4), 261–265.

(51) Khusnutdinova, J. R.; Rath, N. P.; Mirica, L. M. Dinuclear Palladium(III) Complexes with a Single Unsupported Bridging Halide Ligand: Reversible Formation from Mononuclear Palladium(II) or Palladium(IV) Precursors. *Angew. Chem., Int. Ed.* **2011**, *50* (24), 5532–5536.

(52) Based on a search of The Cambridge Crystallographic Data Centre database, August 2019.